Z. Phys. D 40, 282–287 (1997)

ZEITSCHRIFT
FÜR PHYSIK D

Nanowires: size evolution, reversibility, and one-atom contacts

Uzi Landman, R. N. Barnett, W. D. Luedtke

School of Physics, Georgia Institute of Technology, Atlanta, GA 30332, USA

Received: 9 July 1996 / Final version: 12 September 1996

Abstract. Size-evolutionary patterns of mechanical and electronic transport properties in junctions are discussed, showing formation of nanowires upon narrowing, regardless of the initial dimensions of the junctions. Mechanical and conductance reversibility of such nanowires in elongation and compression cycles is studied. Ab-initio local-spin-density functional based molecular dynamics simulations show formation of a stable "one-atom" contact in a sodium wire at 189 K, with the atomic structure near the apex of the nanowire correlated to that of two pentagonal pyramidal Na_7 clusters joined by the apex atom. The average electronic conductance through the one-atom contact, at 189 K, is estimated to be $\sim 4.5\,(2e^2/h)$.

PACS: 71.24.+q; 36.40.Cg

1 Introduction

Physical and chemical properties of materials are expected, and often do, exhibit dependencies on dimensionality and size as well as on thermodynamic state and degree, or form of aggregation. While the ability to change materials properties via variations in particle size has been utilized since antiquity (with examples including pigments prepared by ancient Chinese artisans through grinding or milling, and ink produced in Egypt in the time of the pharos through the dispersion of carbon particles in water), and studied through the centuries (e.g., the preparation and observations by Faraday [1] of gold colloids in 1864, marking the birth of colloid science), it is only in the past two or three decades that systematic investigations of size-evolutionary patterns of materials properties have been carried out. These scientific endeavors, which led to the emergence of cluster science, have unveiled in a number of cases the origins of size-evolutionary patterns of materials physical and chemical properties under various conditions and environments [2].

Most scientific investigations in this field involve the creation and interrogation of isolated, size-selectable clusters in the gas phase, trapped in matrices, or deposited on surfaces, and studies of colloids and nano-size crystallites in solution or as aggregates, where the particles are commonly passivated to inhibit their propensity to agglomerate and sinter [3]. Another class of physical systems which exhibit size-dependent evolutionary patterns, and offer opportunities for systematic investigations of such effects, are junctions (nanowires) which as we will show may contain structural elements which can be regarded in certain circumstances as clusters supported between macroscopic bodies. In Sect. 2 we discuss size-evolutionary patterns in junctions and formation of nanowires upon elongation and narrowing [4–6]. The reversibility of mechanical and conductance characteristics of nanowires [7] are discussed in Sect. 3. We conclude in Sect. 4 with a discussion of the geometry, electronic structure and transport in a "one-atom" junction [8] (one-atom contact), of a sodium nano-wire.

2 Large and small junctions – size evolution

Junctions are materials structures which form upon bringing bodies into proximal interaction, during the separation of contacting bodies, or in the process of extension (e.g., pulling) of a material system. Past, as well as intensifying current, investigations of junctions have been motivated by the ubiquity of circumstances in which they may be formed; either naturally in the course of a physical process (as in the case of materials surfaces brought to close proximity and/or in relative motion with respect to each other where the frictional resistance to shear has been attributed [9] to the formation of interfacial junctions, or as the source of interfacial adhesive action), or intentionally (e.g., controlled generation of wires via the extension of materials contacts, as in the case of surface manipulations using tip-based methods [4–6,10–14], a break-junction technique [15], or by separation of wires in contact [7, 16]). Formation of such nanowires was predicted by early molecular dynamics studies of tip-substrate interactions [4, 5, 17] and subsequent experimental observations [4, 7, 10–16] revealing remarkable properties of such junctions, particularly three-dimensional nanometer scale wires, which are of fundamental as well as of potential technological interest in the areas of miniaturization and very large scale assembly and integration of electronic devices. These findings include: structural characteristics (i.e.,

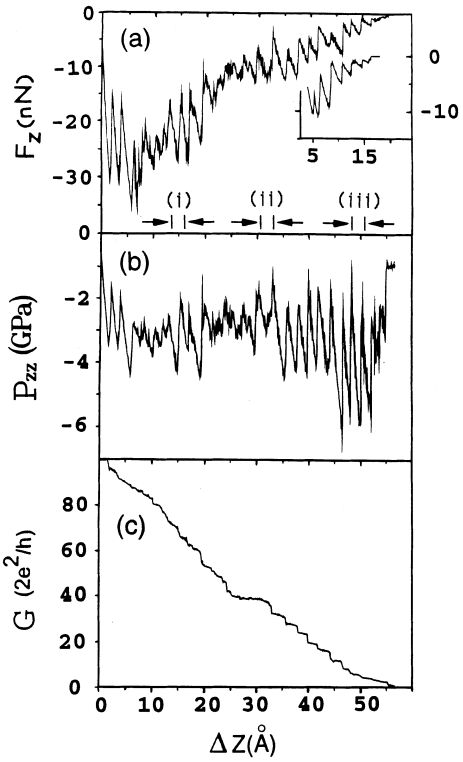

Fig. 1a–c. F_z in nN, shown in **a**, axial component of the stress tensor P_{zz} in GPa, shown in **b** and calculated conductance (G, in unit of $2e^2/h$, shown in **c**, plotted verus displacement Δz, in Å obtained from room-temperature MD simulations of the elongation of a large (111)-oriented gold wire (initially equilibrated as a 30-layer wire with a $\sim$ 17 Å radius of its narrowest cross-section). The displacement intervals marked (*i*)–(*iii*) correspond to those for which atomic configurations are shown in Fig. 1a–c, respectively. Shown in the inset is the force (F_z, in nN) recorded in a separate simulation of the elongation process of smaller Au(111) wire (equilibrated initially as a 16-layer wire with a radius of $\sim$ 10 Å at its narrowest cross-section). The displacement scale for the shorter wire was positioned with respect to that of the longer one such that at its start the radii of the narrowest cross-sections of the two wires achieved very close values. This comparison serves to illustrate the invariance of the properties of nanowires formed during elongation of junctions with respect to the initial sizes of the junctions

crystallinity) [4–6]; mechanical response [4–6, 12, 14], characterized by ideal critical yield stress values, with elongation occurring through a sequence of plastic stress accumulation and relief stages associated with ordered and disordered atomic configuration of the wires, and portrayed in oscillatory behavior of the pulling force; electronic transport [7, 10, 11, 13–16, 18] exhibiting room temperature conductance quantization as well as possible transition to a localization regime in sufficiently long wires [11]; and predictions of magneto-transport effects [19], including magnetic switching and magnetic blockade [20], occurring through the shifting of electronic energy levels in nanowires by an applied longitudinal magnetic field.

It is natural to inquire about the dependence of the formation mechanisms and properties of junctions on their dimensions, and their size evolution [4–6]. To this end we show in Fig. 1 physical characteristics obtained via simulations of the room temperature elongation processes of relatively large junctions. In these simulations two crystalline gold wires oriented with the (111) direction parallel to the axis of the wire were used: (a) a long wire containing 8030 atoms, 5742 atoms trated dynamically and equilibrated initially as a 30-layer wire with the remaining atoms comprising Au(111) substrates of 2 layers each supporting the top and bottom of the wire, and (b) a shorter wire (see inset in Fig. 1a), consisting of 3273 atoms, 1600 atoms treated dynamically and equilibrated initially as a 16-layer wire and the rest comprising Au(111) static substrates. In Fig. 2 we display atomic configurations and short-time trajectories recorded at selected stages of the elongation process of the longer wire (Fig. 2a–c) corresponding to the intervals marked (i)–(iii) in Fig. 1a. From these simulations the following main observations can be made:

(*i*) Underlying the oscillatory sawtooth pattern of the forces in Fig. 1a, and the corresponding behavior of the axial component of the stress tensor (calculated at the narrowest region of the wire) shown in Fig. 1b are the atomistic mechanisms of elongation of the wire. As aforementioned these processes occur via a succession of alternating stress accumulation and relief stages, during which the wire undergoes plastic structural transformations. The atomic structure of the wire is crystalline-ordered in nature during most of the evolution of the wire (though strained during the stress accumulation stages); see for example the left and right configurations in Figs. 2a–c. These ordered states of the wire are interrupted rather abruptly by brief transformation stages during which the wire is locally disordered. For wires as thick as those used in this study these transformations involve multiple-glide processes primarily on (111) glide planes (see Figs. 2a–c); in particular note the middle configurations in Figs. 2a and 2b recorded during the glide stage, where the glide planes are denoted by arrows). The structural transformations lead to elongation of the wire. Accompanying these processes are variations in the cross sectional areas and shapes of the wire; note that the intersection of the glide planes with the periphery of the wire can cause areal and shape changes even in locations other than the narrowest neck region, which in some circumstances can lead to a double-constriction structure. Additionally, for sufficiently thin wires successive narrowings are localized at the narrowest region (typically for wires with diameters < 20 Å, depending on the ratio of the neck radius to the global axial radius of curvature of the wire), while for thicker ones, i.e., at the earlier stages of pulling of a thick wire, narrowings may occur occasionally at thicker regions, leaving the area and shape of the narrowest constriction essentially unaltered.

Since ballistic conductance through the wire is determined mainly by the dimensions and shape of the narrowest constriction (i.e., the number of conducting channels is given by the number of transverse electronic states at this region, and their degeneracies; see Refs. 18, 19 and citations to other studies therein), such occurrances can lead to the development of extended plateaus in the conductance measured versus the extent of elongation. Indeed, such an extended plateau is seen in Fig. 1c (in the interval 25 Å $\leq z \leq$ 32.5 Å), where we display the conductance of the wire calculated via a semiclassical modification of Sharvin's expression [21]. Furthermore, double-constriction structures may also influence the conductance characteristics (e.g., when the two constrictions in a doubly-constricted wire are well separated

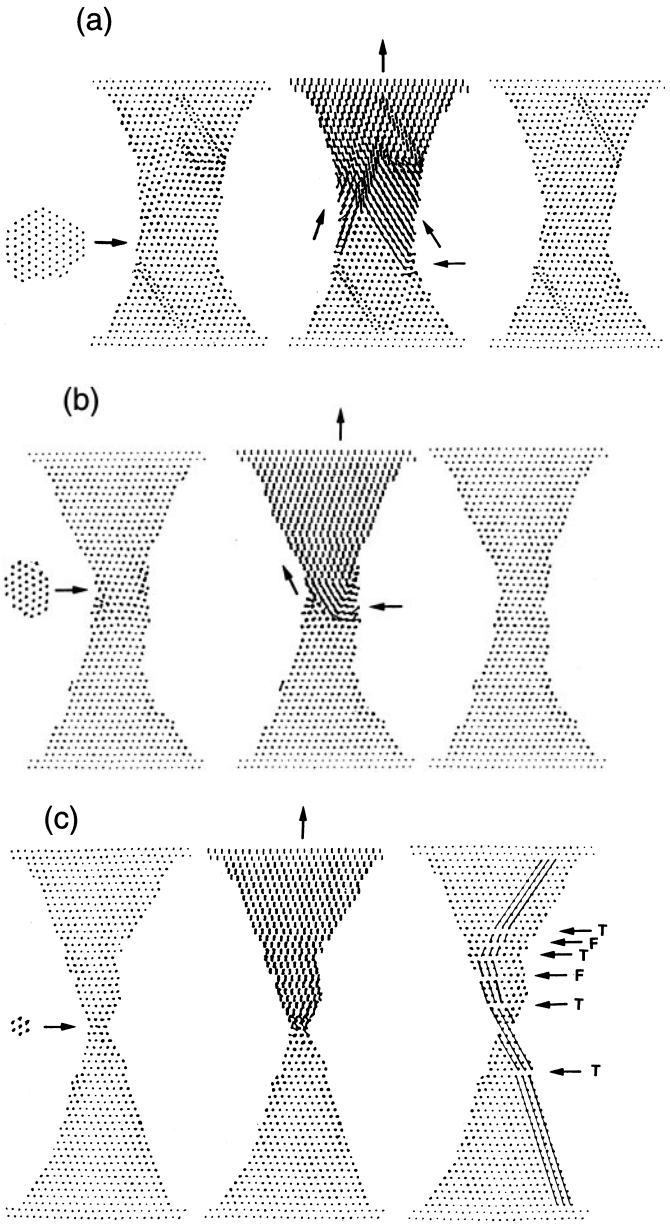

Fig. 2a–c. Side views of atomic configurations and short-time trajectories in 5 Å thick vertical slices through the long wire, recorded **a–c** during the elongation stages (*i*)–(*iii*) marked in Fig. 1, respectively. In each stage the left and right frames correspond to before and after configurations, and the central one corresponds to the brief structural transformation stage (the arrows in the middle frame D denote the glide directions). For the final configuration in **c** fault (F) and twin (T) planes are marked (lines along atomic rows are drawn to guide the eye). Included also in **a–c** are top views of the narrowest cross-sections of the wires, before the elongation step

from each other the total resistance of the wire is that due to two constrictions in series resulting in a smaller conductance).

We also observe that the structural transformations of the wire can lead to the generation of stacking faults and/or twin-boundanries (see for example Fig. 2a). Such defects may anneal during the structural evolution of the pulled wire (compare Figs. 2a and b), and some may be present even in the ultimate stretched nanowire (see Fig. 2c where faults and twin boundaries, denoted by F and T, respectively, are seen). Such defects may also influence the ballistic transport of electrons through the wire. Finally, we note that the local curvature of the axial shape of the pulled wire may be very different from the overall average curvature (see in particular Fig. 2c). The local curvature at the vicinity of the narrowest constriction of the wire influences the tunneling contribution to the transmission through the constriction, and is of importance in estimating the conductance through such wires (see Ref. 19 and citations of earlier studies therein).

(*ii*) The force and axial pressure traces (Fig. 1a,b recorded during elongation of a large wire (equilibrated initially with a constriction radius of 17 Å) exhibit a regular pattern (almost equally spaced oscillations with a period of $\approx$ 2.5 Å; the interlayer distance between (111) layers is $\approx$ 2.35 Å) at the later stages of elongation (i.e., for $\Delta z \geq 32.5$ Å, when the radius of the narrowest constriction in the wire achieved a value of $\approx$ 10 Å). On the other hand, prior to this stage ($\Delta z \leq 32.5$ Å, corresponding to a thicker wire) the force and stress patterns are more irregular, with large variations in the oscillation amplitudes and periods. Underlying this difference in behavior is the observation that when the wire is thicker accumulated stresses induced by pulling may be distributed in various regions of the wire and a large number of glide planes (mainly (111)) with variable dimensions can be active. This leads to a broad variation of the critical stress values from one elongation stage to another. As the wire thins down the stresses concentrate at the narrowest region of the wire and the number of active glide planes decreases, resulting in a more regular pattern of the forces and stresses. This is reflected also in the calculated conductance (Fig. 1c) which shows a much more regular pattern past $\Delta z \approx 32.5$ Å, characterized by well-defined plateaus and step-rises. (Note in this context the small slopes of the semiclassically calculated conductance plateaus originating from variation of the uniaxial strain during the stress accumulation intervals (between yield, i.e., transformation, stages) which is accompanied by continuous contraction of the wire's cross-sectional areas; such slopes have been observed experimentally [7].)

(*iii*) A most interesting result of the simulations pertains to the "universal" nature of the mechanical and electrical properties of junctions. It has been observed already from the early simulations [4, 5] that nano-meter scale wires are formed at the latter stages of elongation irrespective of the initial size of the contact. This is further illustrated in Fig. 1a where the force vs. elongation curves for two wires of different initial dimensions are compared starting from the corresponding elongation stages when the radii of the narrowest cross-sections of the two wires become very close to each other ($\approx$ 8 Å). The similarity between the force curves for the two wires (also reflected in other mechanical characteristics and in the calculated conductance curves, not shown here for the shorter wire) confirms formation of nanowires of similar nature, irrespective of the previous history of the junction. Indeed, such considerations guided recent experiments where quantized conductance in nanowires has been measured via separation of the contact betweeen two macroscopic bodies [7, 16].

3 Reversible manipulations of nanowires

We focus here on recent MD investigations [7] pertaining to the ability to mechanically manipulate and control the quantum conductance in gold nanowires at room temperature. In these simulations a crystalline gold wire oriented with the (111) direction parallel to the axis of the wire and containing 3273 atoms (1600 atoms treated dynamically and equilibrated initially as a 16-layer wire with the remaining atoms comprising Au(111) static substrates of 2 layers each, supporting the top and bottom of the wire), was modeled via the many-body embedded-atom potentials. The wire was elongated by $\sim$ 12 Å (the spacing between adjacent (111) planes is 2.35 Å) and subsequently compressed by the same amount at a rate of 2 m/s (i.e., 0.02 Å/ps) under isothermal conditions at $T = 300$ K. Figure 3a depicts the pulling force (i.e., the force on the holder substrates at the top and bottom of the wire) and Fig. 3b shows J_2, the square-root of the second invariant of the deviatory stress tensor, which is proportional to the stored elastic energy available for shear deformation [4, 22]. In Fig. 3c we display the conductance of the nanowire calculated as before from a semiclassical modification of Sharvin's expression [21]. Side-views of atomic configurations with short-time trajectories recorded at selected stages during the elongation (a–c), and compression (a′–c′) are shown in Fig. 4.

Underlying the oscillatory sawtooth pattern of the forces in Fig. 3a and the corresponding behavior of J_2, is the atomistic mechanism of the elongation and compression of the wire. These processes occur as aforementioned via a succession of alternating stress accumulation and relief stages (concentrating at the narrow section of the wire), during which the wire undergoes plastic structural transformations [4–6]. The nanowire's atomic structure is crystalline-ordered in nature during most of the evolution of the wire (see for example Fig. 4a, c, a′ and c′). However, this structure is strained during the stress accumulation stages, corresponding to the smaller slopes of the sawtooth patterns in Figs. 3a, b. The ordered states of the wire are interrupted rather abruptly by brief transformation (yield) stages during which the wire is locally disordered. For wires as thick as those used in this study these transformations involve multiple glide processes on (111) planes (Fig. 4b, b′), leading to elongation and narrowing (Fig. 4a–c), or shortening and thickening (Fig. 4a′–c′), of the nanowire. As seen from Fig. 3, the mechanical and transport characteristics of the wire during elongation and compression are "phase-shifted" with respect to each other. This effect, which has been observed experimentally [12], is due to the change from tensile to compressive stress upon reversal of the process from elongation to compression, respectively.

It should also be remarked that the force per unit area in the neck region of the wire, obtained from the simulated force or stress records, displays the same general behavior as the overall force (Fig. 3a) and exhibits critical uniaxial stress values of 5 to 6 GPa, which, when resolved along the glide directions yield critical resolved shear stress values of $\sim$ 4 GPa. This value, which is over an order of magnitude larger than that of bulk gold [23], is in approximate agreement with the average value of J_2 for the neck region (Fig. 3b) and is comparable to the theoretical value for Au

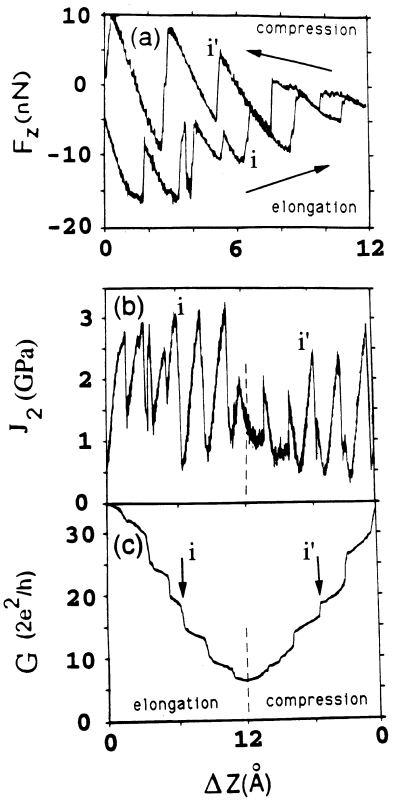

Fig. 3a–c. Force F_z (in nN, shown in **a**), J_2 (in GPa, shown in **b**) and calculated conductance G (in unit of $2e^2/h$, shown in **c**), plotted versus displacement (Δz, in Å) obtained from MD simulations of elongation and compression of a (111) oriented gold nanowire at room temperature. In **a** the records for the elongation and compression stages are folded on the same distance scale, while in **b** and **c** they are plotted side by side with the reversal of the direction taking place at $\Delta z = 12$ Å

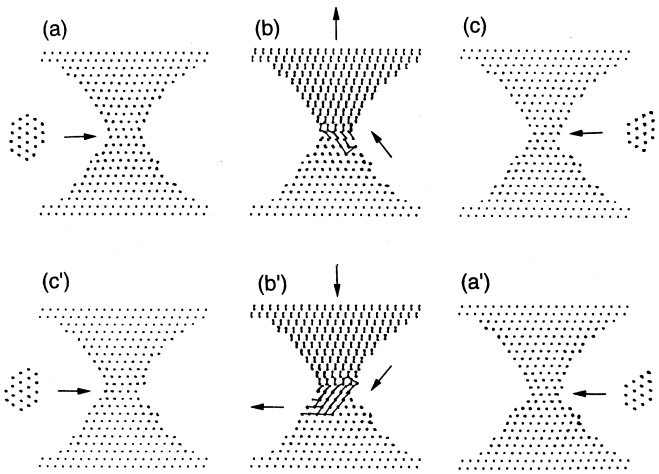

Fig. 4a–c. Side views of atomic configurations and short-time trajectories, in 5 Å thick vertical slices through the wire, recorded during the elongation **a–c** and compression **a′–c′** stages, marked i and i', respectively, in Fig. 3, corresponding to transformation of the Au nanowire from 18 to 19 layers during pulling and the reverse during compression. Frames **a, c** and **a′, c′** correspond to before and after configurations, i.e., a and c′ correspond to a nanowire with 18 layers and **c** and **a′** to 19 layers; included also are top cross-sectional views of the narrowmost region of the wire. Frames b and b' correspond to the fast structural trnsformation stages exhibiting multiple-glide processes (glide directions denoted by *arrows*). In each frame the two atomic layers at top and bottom correspond to the Au substrates supporting the wire

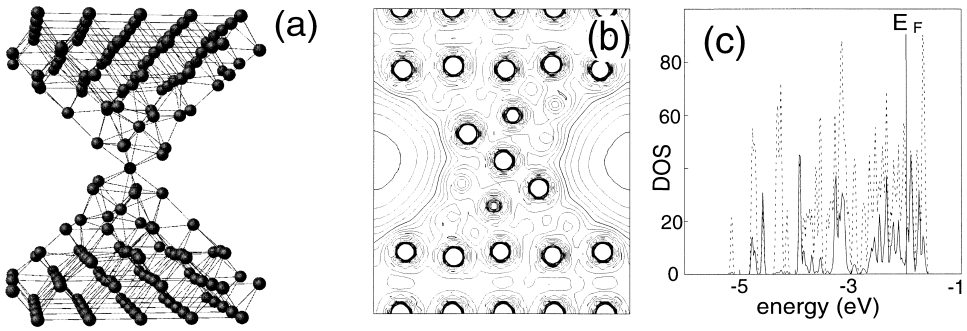

Fig. 5a–c. An optimal configuration of a "one-atom" contact sodium nanowire, obtained via ab-initio simulations. Note the 5-fold rings on both sides of the apex atom, **b** contours of the local part of the self-consistent LSD effective potential (all contours correspond to negative values, and the spacing between contours is 0.025 Hartree; the Fermi energy $E_{\rm F} \approx -0.075$ Hartree corresponds to the 4th contour from the *right*, or *left*). Note the spatial extent of the potential at the narrowing. **c** Local (*solid*) and total (*dashed*) density of states; $E_{\rm F}$ is marked by a *vertical line*

(1.5 GPa) in the absence of dislocations [23], as well as being close to our earlier theoretical predictions [4] which were confirmed by experiments [12c, 24]. The mechanical "ideal" nature of the nanowires, which can be related to their characteristic small dimensions and the inability to support dislocation sources (e.g., Frank-Read sources [25]), are correlated with the observed reversibility of their properties [26].

The calculated [21] conductance (Fig. 3c) portrays the structural variations in the nanowire, and each of the step-rises correlates directly with the signatures of the structural transformations (compare Fig. 3c with 3a, b). Furthermore, the variation of the uniaxial strain during the stress accumulation intervals (between yield, i.e., transformation, stages) is accompanied by continuous contractions and expansions of the whire's cross-sectional areas for the elongation and compression cycles, respectively. This is reflected in the slopes of the conductance plateaus, in both the calculations and recent experimental results using a pin-plate set-up, which exhibit clear room-temperature reversibility in long conductance traces [7].

4 Single atom contacts

As already found in our earlier studies [4] the ultimate stage of elongation (prior to breaking of the junction) may lead to formation of a single-atom contact between the two parts of the nanowire. This structure, referred to also as single-atom point contact, offers new unique possibilities for investigations of electronic phenomena involving atomic-scale contacts between macroscopic bodies [27]. To further investigate the structural, dynamic and electronic properties of such unique structures we have initiated studies using the Born-Oppenheimer Local-Spin-Density Functional Molecular-Dynamics (BO-LSD-MD) method [28] in investigations of simple metal (sodium) nanowires. In these calculations a supercell of 19.98 Å$\times$19.98 Å$\times$23.97 Å dimensions was used, with non-local norm-conserving pseudo-potentials for sodium and a plane wave cutoff energy of 6.2 Ry. In dynamical simulations a time-step of 3 fs was used.

An optimized structure of a sodium nanowire consisting of 144 atoms (119 treated dynamically) formed between two sodium surfaces separated by 23.97 Å is shown in Fig. 5a. The local part of the effective potential corresponding to this structure determined through self-consistent solution of the Kohn-Sham equations, is shown in Fig. 5b; note that the width of the confining potential near the one-atom narrowing is larger than atomic size. This structure developed dynamically in simulations at $T = 189$ K, starting from a tapered sodium wire consisting of stacked (100) layers, supported by two Na(100) surfaces separated by 23.97 Å. The first remarkable observation is that such a "single-atom" junction is indeed energetically stable. The second imortant, and at first surprising, observation pertains to the specific atomic arrangement near the apex of the nanowire. As seen from Fig. 5a the structure in that region consists of two close to parallel five-fold atomic rings and a single atom between them (i.e., two pentagonal pyramids with a shared apex). Interestingly, this structure is reminiscent of atomic configurations of gas-phase sodium clusters with the optimal one for Na_6 consisting of a pentagonal pyramid, and that for Na_7 consisting of two base sharing pentagonal pyramids; alternatively it may be described as a 13-atom icosahedron. Evidently the "rarefied" environment in the vicinity of the narrowing of the nanowire stabilizes a structure derived from, and in direct correlation with, that of isolated clusters. It is also important to note that in dynamical simulations of the wire at 189 K the structure fluctuates without losing its characteristic features.

The time dependence of the extrapolated electrical conductance of the nanowire ($G(\omega \to 0)$), calculated during a 3 ps simulation via the Green-Kubo expression

$$\sigma(\omega) = \frac{2\pi e^2}{m^2 \omega \Omega} \sum_{ij} (f_i - f_j) |\langle \psi_i | P_z | \psi_j \rangle|^2 \delta(E_i - E_j - \hbar\omega) \,,$$

[where e and m are the charge and mass of the electron, P_z is the momentum operator, ψ_i and E_i are the electronic LSD eigenfunctions and eigenvalues (with corresponding occupation numbers f_i), and Ω is the volume of the calculational cell; we should note that in our BO-LSD-MD method [28] the occupancies of the levels are governed by the Fermi distribution, thus allowing partial occupancies], is shown in Fig. 6a, along with the time dependence of the total and local (centered on the apex region) densities of states at the Fermi level (see density of states for the optimal configuration in Fig. 5c). From the time average (over ionic configurations) of G, obtained via extrapolation of $\sigma(\omega)$ to $\omega = 0$ and using

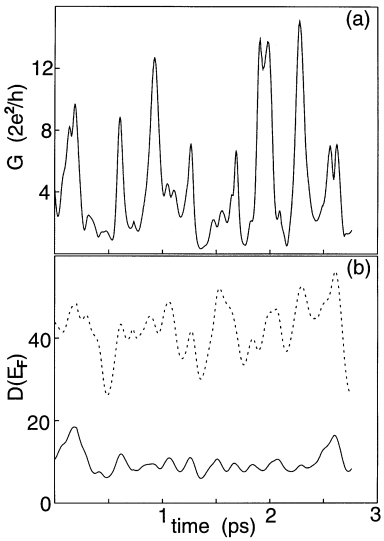

Fig. 6a,b. Time dependence of the extrapolated conductance $G(\omega \to 0)$ (in units of $2e^2/h$), and of the density of states at the Fermi-level, $D(E_{\rm F})$, obtained during BO-LSD-MD simulations. The time average of G yields the result quoted in the text

the total length $L = 23.97$ Å and area $S = 399$ Å^2 of the computational cell, we estimate that the average conductance of the nanowire $\langle G\rangle = \langle\sigma\,(\omega \to 0)\rangle\; S/L \approx 4.51\,(2e^2/h)$, i.e., a resistance $R \simeq 2.86\,{\rm k}\Omega$. It is interesting to note that the thermal fluctuations of the conductance of the wire correlate with those in the density of state near the Fermi level (see Fig. 6) and with thermal vibrations of the structure (mainly in the vicinity of the narrowing), occurring on a subpicosecond time scale. These observations suggest that measurements of electrical transport through such junctions could provide new insights pertaining to the atomic dynamics and the nature of transport in these structures, as well as issues related to switching phenomena [20, 29].

This work is supported by the U.S. Department of Energy and the U.S. Air Force Office for Scientific Research. Computations were performed on CRAY computers at the National Energy Research Supercomputer Center, Livermore, CA, the Pittsburgh Supercomputing Center, and at the GIT Center for Computational Materials Science.

References

1. Faraday, M.: Phil. Trans. R. Soc. London **147**, 145 (1857)
2. See articles in: Clusters of Atoms and Molecules, edited by H. Haberland, Springer Series in Chem. Phys., vols. 52 and 57. Berlin: Springer 1994
3. Whetten, R.L., Khoury, J.T., Alvarez, M., Murthy, S., Vezmar, I., Wang, Z.L., Stephens, P.W., Cleveland, C.L., Luedtke, W.D., Landman, U.: Adv. Mater **8**, 428 (1996); Luedtke, W.D., Landman, U.: J. Phys. Chem. **100**, 13323 (1996)
4. Landman, U., Luedtke, W.D., Burnham, N.A., Colton, R.J.: Science **248**, 454 (1990)
5. Landman, U., Luedtke, W.D.: J. Vac. Sci. Technol. B **9**, 414 (1991)
6. Landmann, U., Luedtke, W.D., Gao, J., Langmuir **12**, 4514 (1996)
7. Landman, U., Luedtke, W.D., Salisbury, B.E., Whetten, R.L.: Phys. Rev. Lett. **77**, 1362 (1996)
8. Barnett, R.N., Landman, U.: to be published
9. (a) Bowden, E.P., Tabor, D.: Friction (Anchor Press/Doubleday, Garden City, N.Y. 1973); (b) For a recent review see Bushan, B., Israelachvili, J.N., Landman, U.: Nature **374**, 607 (1995)
10. Pascual, J.I., Mendez, J., Gomez-Herrero, J., Baro, A.M., Garcia, N., Vu Thien Binh: Phys. Rev. Lett. **71**, 1852 (1993)
11. Pascual, J.I., Mendez, J., Gomez-Herrero, J., Baro, A.M., Garcia, N., Landman, U., Luedtke, W.D., Bogachek, E.N., Cheng, H.-P.: Science **267**, 1793 (1995); J. Vac. Sci. Technol. B **13**, 1280 (1995)
12. (a) Agrait, N., Rodrigo, J.G., Vieira, S.: Phys. Rev. B **47**, 12345 (1993); (b) Agrait, N., Rodrigo, J.G., Cirvent, C., Vieira, S.: Phys. Rev. B **48**, 8499 (1993); (c) Agrait, N., Rubio, G., Vieira, S.: Phys Rev. Lett **74**, 3995 (1995)
13. Olesen, L., Laegsgaard, E., Stensgaard, I., Besenbacher, F., Schiotz, J., Stoltze, P., Jacobsen, K.W., Norskov, J.N.: Phys. Rev. Lett. **72**, 2251 (1994)
14. Stalder, A., Durig, U.: Appl. Phys. Lett. **68**, 637 (1996)
15. Krans, J.M., van Ruitenbeek, J.M., Fisun, V.V., Yanson, I.K., de Jongh, L.J.: Nature **375**, 767 (1995), and references to earlier work therein
16. Costa-Kramer, J.L., Garcia, N., Garcia-Mochales, P., Serena, P.A.: Surface Science **342**, L 1144 (1995)
17. Landman, U., Luedtke, W.D., Ribarsky, M.W.: J. Vac. Sci. Technol. A **7**, 2829 (1989)
18. Bogachek, E.N., Zagoskin, A.M., Kulik, I.O.: Fiz. Nizk. Temp. **16**, 1404 (1990) [Sov. J. Low Temp. Phys. **16**, 796 (1990)]
19. Scherbakov, A.G., Bogachek, E.N., Landman, U.: Phys. Rev. B **53**, 4054 (1996)
20. Bogachek, E.N., Scherbakov, A.G., Landman, U.: Phys. Rev. B **53**, 13246 R (1996)
21. Fal'ko, V.I., Lesovik, G.B.: Sol. Stat. Commun. **84**, 835 (1992); Torres, J.A., Pascual, J.I., Saenz, J.J.: Phys. Rev. B **49**, 16581 (1994). The calculation of the conductance uses a modified Sharvin expression which is based on Weyl's theorem (see e.g. Morse, P.M., Feshbach, H.: Methods of Theoretical Physics (McGraw-Hill, New York, 1953, p. 761), relating the number of transverse states (channels) in the narrowest part of the junction to the corss-sectional area and the circumference of the narrowing. These quantities were estimated from the geometries of atomic wire configurations obtained during the simulation. Due to strong screening in metals the effective potential confining the electrons in the wire is short-ranged (as also found in recent local density functional calculations of metallic wires by R.N. Barnett and U. Landman, ref. 8) approximating well a hard-wall boundary potential, corresponding to the Dirichlet boundary condition used in derivation of the Weyl theorem
22. Dieter, G.: Mechanical Metallurgy (McGraw-Hill, New York, 1967); see also Landman, U:, Luedtke, W.D., Ringer, E.M., in: Fundamentals of Friction, eds. Singer, J.L., Pollock, H.M. (Kluwer, Dordrecht, 1991), p. 463
23. Kelly, A., MacMillan, N.H.: Strong Solids (Clarendon, Oxford, 1986)
24. Apparent pressures in the range of 3 to 6 GPa measured for Au nanowires at 300 K, in agreement with our earlier [4] and current predictions, have been reported most recently, see Rubio, G., Agrait, N., Vieira, S.: Phys. Rev. Lett. **76**, 2302 (1996)
25. Hall, D.: Introduction to Dislocations (Pergamon, Oxford, 1975)
26. For early studies on whiskers, see: Herring, C., Galt, J.K.: Phys. Rev. **85**, 1060 (1952)
27. For other theoretical studies of conductance in nanowires and point contacts see: (a) Lang, N.D.: Phys. Rev. B **52**, 5335 (1995), and references therein to earlier work by the author, including studies of a single atom point source for electrons, Lang, N.D., Yacoby, A., Imry, Y.: Phys. Rev. Lett. **63**, 1499 (1989), and resistance of a one-atom contact in the scanning tunneling microscope, Lang, N.D.: Rev. B **36**, 8173 (1987); (b) Bartkovsky, A.M., Sutton, A.P., Todorov, T.N.: Phys. Rev. B **52**, 5036 (1995); (c) Brandbyge, M., Schiotz, J., Sorensen, M.R., Stoltze, P., Jacobsen, K.W., Norskov, J.K., Olesen, L., Laegsgaard, E., Stensgaard, I., Besenbacher, F.: Phys. Rev. B **52**, 8499 (1995)
28. Barnett, R.N., Landman, U.: Phys. Rev. B **48**, 2081 (1993)
29. Smith, D.P.E.: Science **269**, 371 (1995)